Journal of Theoretical and Computational Acoustics
Vol. 31, No. 1 (2023) 2350001 (29 pages)

DOI: 10.1142/S2591728523500019

A Frequency-Domain Formulation for Predicting Multi-Frequency Noise Generated by Flows with Periodically Moving Boundaries

Zhiteng Zhou*, Hongping Wang†, Zhenyu Zang‡ and Shizhao Wang§

Institute of Mechanics, Chinese Academy of Sciences
Beijing 100190, P. R. China

School of Engineering Sciences
University of Chinese Academy of Sciences
Beijing 100049, P. R. China
**zhouzhiteng18@mails.ucas.ac.cn*
†*hpwang@imech.ac.cn*
‡*zangzhenyu@imech.ac.cn*
§*wangsz@lnm.imech.ac.cn*

Received 12 February 2022
Revised 6 September 2022
Accepted 4 December 2022
Published 19 January 2023

A frequency-domain formulation is proposed to compute the far-field noise generated by flows with periodically oscillating or rotating boundaries. The proposed formulation significantly enhances the efficiency of the frequency-domain method in handling the multi-frequency sources with nonrectilinear motion. The novelty of the proposed method is that the frequency- and time-dependent components of the Ffowcs Williams and Hawkings (FW-H) integral are separated by using the far-field asymptotic Green's function. The separation of the frequency- and time-dependent components avoids the need for an expensive time integration in computing the multi-frequency noise generated by flows with periodically moving boundaries. They proposed only one Fourier transform computation in obtaining the noise at different frequencies. The efficiency of the proposed formulation is investigated by analyzing the required number of floating-point operations. Its validity is examined by computing the noise from rotating or oscillating permeable boundaries around composite monopoles and a flapping wing. The proposed formulation is applicable to the FW-H integral with periodically oscillating or rotating boundaries when the maximum velocity on the moving boundary is subsonic.

Keywords: Ffowcs Williams and Hawkings integral; broadband noise; multi-frequency noise; frequency-domain formulation; moving boundaries.

§Corresponding author.

1. Introduction

Aerodynamic noise prediction is an important issue in engineering applications.[1–5] The Ffowcs Williams and Hawkings (FW-H) equation is widely used for predicting aerodynamically generated noise. This inhomogeneous wave equation[6] is derived from the extension of Lighthill's acoustic analogy equation[7] for problems with moving boundaries. The solution of the FW-H equation reflects the process of acoustic radiation, in which the effects of moving boundaries are represented by moving sources in the inhomogeneous wave equation.

Various types of time-domain formulations[8,9] and frequency-domain formulations[10,11] have been proposed to solve the FW-H equation. Time-domain formulations have been successfully used to predict tonal or broadband noise generated from flows with fixed boundaries,[2,12] and moving boundaries.[4,13–15] However, the application of frequency-domain formulations to problems with moving boundaries is usually limited to predicting the tonal noise, where only the noise at specific frequencies is computed.[16] The use of these frequency-domain formulations in predicting multi-frequency or broadband noise is computationally expensive due to the time integral computation for each frequency in the broadband.[16]

Gennaretti *et al.*[17] proposed a frequency-domain formulation based on frequency-response-function matrices to predict the multi-frequency tonal noise generated by rotors in arbitrary steady motion. The proposed formulation is derived from "Formulation 1A" for the solution of the FW-H equation.[8] Fully populated transfer function matrices are constructed to relate the source noise harmonic to the far-field observer noise harmonics. This formulation has the advantage of identifying the featured radiated sound from each specific single-harmonic input. For a given single-harmonic input source noise, the proposed formulation outputs the multi-harmonic noise signals at the observer points. The approach of Gennaretti *et al.*[17] has been successfully applied to compute multi-frequency noise generated by steady rotating boundaries in arbitrary forward motion and is applicable to rotor configurations from which the tonal noise is much higher than the broadband noise.

Lockard[10] proposed a frequency-domain formulation that has the capability to efficiently compute the broadband noise generated from flows with subsonic moving boundaries. The formulation proposed by Lockard[10] is efficient in computing the broadband noise because the time integral is not computed for each frequency. This method is derived from a Galilean transformation, where the problem of uniform rectilinear motion of boundaries and observers in a medium at rest is transformed to the problem of stationary boundaries and fixed observers in a moving medium. The formulation is valid when the observers are at rest relative to the boundaries. Bozorgi *et al.*[18] then reformulated the problem by defining a reference frame that moves with the boundary, resulting in a problem with a stationary boundary and a movable observer in a moving medium. These formulations have been validated for the case of noise generated by flows with rectilinearly moving boundaries. However, they are not applicable to problems with rotating or oscillating boundaries.

The aim of this work is to propose a frequency-domain formulation that can efficiently compute the multi-frequency or broadband noise generated by flows with periodically oscillating or rotating boundaries. The proposed frequency-domain formulation is based on the

framework developed by Lockard[10] and Bozorgi *et al.*,[18] which can efficiently compute multi-frequency and broadband noise. We focus on the problem of a fixed observer in an ambient medium at rest. The periodically moving boundary can be permeable or nonpermeable. The motion of the boundaries is either periodically oscillating or rotating. We do not consider combined rectilinear and oscillating/rotating motion in this work, except when the rectilinear motion is negligible and the Green's function for the convective wave equation can be approximated by that for the standard wave equation.

Compared with conventional frequency-domain formulations, the proposed formulation provides an efficient means of computing the multi-frequency noise or broadband noise. The novelty is that we utilize the asymptotic Green's function to separate the frequency- and time-dependent components of the FW-H integral and to circumvent the expensive time integral computation for each frequency. The required floating-point operations for different formulations are analyzed in detail to clarify the efficiency of the proposed formulation. Our formulation is applicable to both two-dimensional (2D) and three-dimensional (3D) problems with periodically oscillating or rotating boundaries. We must point out that the discussion in this work focuses on a comparison of the efficiency of the proposed method and that of the conventional frequency-domain method. We do not discuss the advantages and disadvantages of the frequency- and time-domain formulations, because it is well known that the frequency-domain method is more efficient than the time-domain method in computing the noise generated by 2D flows.[11] Readers are referred to the work of Lockard,[19] which presents a detailed comparison between the efficiency of a frequency- and time-formulations.

The remainder of this paper is organized as follows. The FW-H equation in the frequency domain is briefly formulated in Sec. 2. Details of the proposed frequency-domain formulation are given in Sec. 3. The proposed formulation is validated in Sec. 4. Finally, the conclusions to this study are presented in Sec. 5.

2. Governing Equations

We begin with the frequency-domain FW-H equation, which is given by[10]

$$\frac{(\mathrm{i}\omega)^2}{c_0^2}\mathcal{F}(p'H(f)) - \frac{\partial^2\mathcal{F}(p'H(f))}{\partial y_i \partial y_i} = \frac{\partial^2\mathcal{F}(T_{ij}H(f))}{\partial y_i \partial y_j} + \mathrm{i}\omega\mathcal{F}(Q) - \frac{\partial}{\partial y_i}\mathcal{F}(F_i), \tag{1}$$

where

$$\begin{aligned} T_{ij} &= \rho v_i v_j + P_{ij} - c_0^2\rho'\delta_{ij}, \\ F_i &= (P_{ij} + \rho v_i(v_j - V_j))n_j, \\ Q &= (\rho(v_i - V_i) + \rho_0 V_i)n_i. \end{aligned} \tag{2}$$

Hereafter, we follow the Einstein's index notation. The FW-H equation is formulated in Cartesian coordinate system. The Cartesian coordinates and time are denoted as y_i and t, respectively. The acoustic pressure waves are assumed to propagate without being affected

by advection. The Lighthill stress tensor is denoted as T_{ij} in which $P_{ij} = (p - p_0)\delta_{ij} - \tau_{ij}$ is the compressive stress tensor, δ_{ij} is the Kronecker delta function and τ_{ij} is the viscous stress tensor. The density, sound speed and pressure in the undisturbed medium are represented by ρ_0, c_0 and p_0, respectively. The density and pressure in the flow field are denoted as ρ and p, respectively. The fluctuations of density and pressure are defined as $\rho' = \rho - \rho_0$ and $p' = p - p_0$, respectively. A physical or permeable boundary of the moving sources is defined by $f = 0$ where f is a signed distance function. The outward unit normal vector on the boundary is denoted as n_i. The Heaviside function is $H(f)$ and the Dirac delta function $\delta(f)$. The ith components of the flow velocity and boundary moving velocity are represented by v_i and V_i, respectively. The Fourier transform of $q(t)$ is denoted as $\mathcal{F}(q(t))$. The Fourier transform pairs used in this work are defined as

$$\mathcal{F}(q(t)) = q(\omega) = \int_{-\infty}^{\infty} q(t) e^{-\mathrm{i}\omega t} \mathrm{d}t,$$

$$\mathcal{F}^{-1}(q(\omega)) = q(t) = \frac{1}{2\pi} \int_{-\infty}^{\infty} q(\omega) e^{\mathrm{i}\omega t} \mathrm{d}\omega.$$

In Eq. (1), the surface defined by $f = 0$ varies with time. Therefore, $H(f)$ and $\delta(f)$ should be considered in the Fourier transform.

3. Solution of the FW-H Equation in the Frequency Domain

By using the frequency-domain Green's function for the wave equation in free space, the solution of Eq. (1) can be given as follows.

$$p'(\mathbf{x}, \omega) H(f) = I_{\mathrm{T}}(\mathbf{x}, \omega) + I_{\mathrm{L}}(\mathbf{x}, \omega) + I_{\mathrm{Q}}(\mathbf{x}, \omega), \tag{3}$$

where

$$\begin{aligned} I_{\mathrm{T}}(\mathbf{x}, \omega) &= \int_{-\infty}^{\infty} \mathrm{i}\omega \mathcal{F}(Q\delta(f)) G \, \mathrm{d}\mathbf{y}, \\ I_{\mathrm{L}}(\mathbf{x}, \omega) &= -\int_{-\infty}^{\infty} \frac{\partial}{\partial y_i} \mathcal{F}(F_i \delta(f)) G \, \mathrm{d}\mathbf{y}, \\ I_{\mathrm{Q}}(\mathbf{x}, \omega) &= \int_{-\infty}^{\infty} \frac{\partial^2}{\partial y_i \partial y_j} \mathcal{F}(T_{ij} H(f)) G \, \mathrm{d}\mathbf{y}, \end{aligned} \tag{4}$$

are the thickness, loading and quadrupole terms of the solution, respectively. Farassat used thickness and loading rather than monopole and dipole because the radiation patterns computed by using the first and second lines in Eq. (4) are different from stationary monopoles and dipoles.[20] The thickness and loading noise equation can be obtained with an impermeable FW-H surface. Although we consider a permeable FW-H surface here, we follow the terminology used by Farassat.[20]

The positions of the observer and source are denoted as $\mathbf{x}$ and $\mathbf{y}$, respectively. The Green's function of the wave equation in the frequency domain is denoted as $G(\mathbf{x}, \mathbf{y}, \omega)$. We

ignore the contributions of the quadrupole term in accordance with the work of Lockard[10] and Bozorgi *et al.*[18] Although the quadrupole source term decays rapidly as the Mach number decrease, the quadrupole sources outside the FW-H surface might generate nonnegligible spurious sound. We assumed that the flow Mach number is sufficiently low or the permeable surfaces for the FW-H equation are large enough to include all relevant quadrupole sources. A quadrupole correction model for estimating the contribution from quadrupole sources outside the FW-H surface might be necessary for some formulations when strong quadrupole sources are convected across the integral surface.[21–24]

3.1. *Computation of the thickness term*

The thickness term in Eq. (3) can be expressed as follows:

$$I_{\mathrm{T}}(\mathbf{x},\omega)=\int_{-\infty}^{\infty}\int_{-\infty}^{\infty}\mathrm{i}\omega Q\delta(f)Ge^{-\mathrm{i}\omega t}\mathrm{d}\mathbf{y}\mathrm{d}t. \tag{5}$$

By using the sifting property of the Dirac delta function $\delta(f)$, the spatial integral in Eq. (5) can be reformulated as the integral on the surface (or contour) $f=0$, that is

$$I_{\mathrm{T}}(\mathbf{x},\omega)=\int_{-\infty}^{\infty}\int_{f=0}\mathrm{i}\omega QGe^{-\mathrm{i}\omega t}\mathrm{d}l\mathrm{d}t, \tag{6}$$

where the differential $\mathrm{d}l$ is the limitation of the discretized element on the integral surface (or contour) $f=0$. Note that $\mathrm{d}l$ is the limitation of length or area of the 2D or 3D discretized element. The Green's function is different for 2D and 3D problems.

Equation (6) is a conventional frequency-domain formulation for noise generated by the thickness term, and enables efficient computations of tonal noise at a given frequency.[16] For example, to compute the tonal noise at $\omega=\omega_1$, one only needs to transform the variable $\mathrm{i}\omega_1 Q(\mathbf{y},t)G(\mathbf{x},\mathbf{y},\omega_1)$ into the frequency domain and compute the spatial integral over the surface $f=0$. The Green's function $G(\mathbf{x},\mathbf{y},\omega_1)$ depends on the given frequency ω_1. One must compute the Fourier transform N times for $\mathrm{i}\omega_i Q(\mathbf{y},t)G(\mathbf{x},\mathbf{y},\omega_i)$ $(i=1,2,\ldots,N)$ for noise with N given frequencies. Therefore, the computation is inefficient if Eq. (6) is directly used to evaluate the multi-frequency or broadband noise where a large number of frequency samples need to be computed.

We propose a frequency-domain formulation that circumvents the difficulties encountered by Eq. (6) to compute the multi-frequency or broadband noise. The proposed frequency-domain formulation can efficiently compute the far-field multi-frequency or broadband noise generated by the thickness term. As will be discussed later, the Fourier transform only needs to be computed once in the proposed formulation to obtain the noise at different frequencies. For convenience, the discussion focuses on 2D flows, which are quite difficult to compute using the time-domain formulations due to the long tail of the Green's function.[11] The 3D version of the proposed method can be directly obtained by replacing the 2D Green's function with the 3D Green's function. We will give the formulations for 3D flows at the end of this section.

The far-field asymptotic form of the 2D Green's function for the wave equation in free space is[11]

$$G(\mathbf{x},\mathbf{y},\omega) \approx -\frac{\mathrm{i}}{4}\left(\frac{2c_0}{\pi\omega R}\right)^{1/2} e^{\mathrm{i}\left(\frac{\pi}{4}-\frac{\omega R}{c_0}\right)}, \quad R=|\mathbf{x}-\mathbf{y}|. \tag{7}$$

The asymptotic form must satisfy the assumption that the observer is far away from the sources ($|\mathbf{x}| \gg |\mathbf{y}|$) and $\omega|\mathbf{x}-\mathbf{y}|/c_0 \gg 1$.[11]

The far-field noise generated by the thickness term given by Eq. (6) can be expressed as

$$I_{\mathrm{T}}(\mathbf{x},\omega) = \int_{-\infty}^{\infty}\int_{f=0} \mathrm{i}\omega Q\left(-\frac{\mathrm{i}}{4}\left(\frac{2c_0}{\pi\omega R}\right)^{1/2} e^{\mathrm{i}\left(\frac{\pi}{4}-\frac{\omega R}{c_0}\right)}\right) e^{-\mathrm{i}\omega t}\mathrm{d}l\mathrm{d}t. \tag{8}$$

The term $-\frac{\mathrm{i}}{4}\left(\frac{2c_0}{\pi\omega}\right)^{1/2} e^{\frac{\mathrm{i}\pi}{4}}$ in Eq. (8) depends only on the frequency ω. Therefore, Eq. (8) can be rearranged as

$$I_{\mathrm{T}}(\mathbf{x},\omega) = \frac{1}{4}\left(\frac{2\omega c_0}{\pi}\right)^{1/2} e^{\frac{\mathrm{i}\pi}{4}} \int_{-\infty}^{\infty}\int_{f=0} \left(\frac{1}{R}\right)^{1/2} Q e^{-\mathrm{i}\omega(t+R/c_0)}\mathrm{d}l\mathrm{d}t. \tag{9}$$

We introduce a new temporal variable $\tau = t + R/c_o$ and rewrite Eq. (9) as

$$I_T(\mathbf{x},\omega) = \frac{1}{4}\left(\frac{2\omega c_o}{\pi}\right)^{1/2} e^{\frac{\mathrm{i}\pi}{4}} \int_{-\infty}^{\infty}\int_{f=0} \frac{Q}{1+M_R}\left(\frac{1}{R}\right)^{1/2} e^{-\mathrm{i}\omega\tau}\mathrm{d}l\mathrm{d}\tau, \tag{10}$$

where $M_R = \frac{1}{c_o}\frac{\mathrm{d}R}{\mathrm{d}t}$ is the Mach number of the source in the direction pointing toward the observer. Note that the substitution of the time variable will not affect the spatial integral although the integral boundary is time-dependent.

Equation (10) is the proposed frequency-domain formulation for the thickness term. It is emphasized that the Fourier transform of $\frac{Q\left(\mathbf{y},\tau\right)}{1+M_R}\left(\frac{1}{R}\right)^{1/2}$ only needs to be computed once using Eq. (10) to obtain the noise at different frequencies. Therefore, compared with the conventional frequency-domain formulation of Eq. (6), the proposed formulation in Eq. (10) is much more efficient in computing multi-frequency or broadband noise.

To compute the noise generated by 3D flows, the Green's function in Eq. (7) should be replaced by

$$G(\mathbf{x},\mathbf{y},\omega) = \frac{1}{4\pi R} e^{-\frac{\mathrm{i}\omega R}{c_0}}. \tag{11}$$

The 3D form of the proposed frequency-domain formulation for computing the noise generated by the thickness term is as follows:

$$I_{\mathrm{T}}(\mathbf{x},\omega) = \frac{\mathrm{i}\omega}{4\pi}\int_{-\infty}^{\infty}\int_{f=0} \frac{Q}{1+M_R}\frac{1}{R} e^{-\mathrm{i}\omega\tau}\mathrm{d}S\mathrm{d}\tau. \tag{12}$$

3.2. *Computation of the loading term*

The loading term in Eq. (4) can be expressed as follows:

$$I_{\mathrm{L}}(\mathbf{x},\omega)=\int_{-\infty}^{\infty}\int_{-\infty}^{\infty}-\frac{\partial(F_i\delta(f))}{\partial y_i}Ge^{-\mathrm{i}\omega t}\mathrm{d}\mathbf{y}\mathrm{d}t. \tag{13}$$

Through integration by parts and using the sifting property of the Dirac delta function $\delta(f)$, we obtain

$$I_{\mathrm{L}}(\mathbf{x},\omega)=\int_{-\infty}^{\infty}\int_{f=0}\frac{\partial G}{\partial y_i}F_ie^{-\mathrm{i}\omega t}\mathrm{d}l\mathrm{d}t. \tag{14}$$

Equation (14) is a conventional frequency-domain formulation for noise generated by the loading term, which allows the efficient computation of the tonal noise at a given frequency.[16] Similar to the conventional frequency-domain formulation for the thickness term given by Eq. (6), this formulation for the loading term requires the Fourier transform to be computed N times for $F_j\frac{\partial G(\mathbf{x},\mathbf{y},\omega_i)}{\partial y_j}$ $(i=1,2,\ldots,N)$ in the case of noise with N given frequencies. Therefore, the direct use of Eq. (14) to evaluate multi-frequency or broadband noise is inefficient.

We propose the following formulation to circumvent the difficulties encountered by Eq. (14) and to efficiently compute the far-field multi-frequency noise generated by the loading term. The far-field asymptotic form of the Green's function can be derived from Eq. (7) as follows[25]:

$$\frac{\partial G}{\partial y_i}\approx\frac{-\omega(y_i-x_i)}{4c_0R}\left(\frac{2c_0}{\pi\omega R}\right)^{1/2}e^{\mathrm{i}\left(\frac{\pi}{4}-\frac{\omega R}{c_0}\right)}. \tag{15}$$

Equation (15) must satisfy the assumption that the observer is far away from the sources ($|\mathbf{x}|\gg|\mathbf{y}|$) and that the wave number is much greater than the reciprocal of the distance ($\omega/c_0\gg 1/|\mathbf{x}-\mathbf{y}|$). Terms of the order $o((1/R)^{1/2})$ are neglected when differentiating the Green's function. Several detailed derivations have been presented.[23–25] Similar to the derivation of Eq. (10), by substituting Eq. (15) into Eq. (14) and introducing the new temporal variable $\tau=t+R/c_0$, we obtain the following formulation:

$$I_{\mathrm{L}}(\mathbf{x},\omega)=\frac{-1}{4}\left(\frac{2\omega}{\pi c_0}\right)^{1/2}e^{\frac{\mathrm{i}\pi}{4}}\int_{-\infty}^{\infty}\int_{f=0}\frac{F_i(y_i-x_i)}{1+M_R}\left(\frac{1}{R}\right)^{3/2}e^{-\mathrm{i}\omega\tau}\mathrm{d}l\mathrm{d}\tau. \tag{16}$$

Equation (16) is the proposed frequency-domain formulation for the loading term. Similar to Eq. (10), the Fourier transform of $\frac{F_i(y_i-x_i)}{1+M_R}\left(\frac{1}{R}\right)^{3/2}$ only needs to be computed once to obtain the noise at different frequencies. Therefore, compared with the conventional frequency-domain formulation of Eq. (14), the proposed formulation in Eq. (16) is much more efficient for computing multi-frequency or broadband noise generated by the loading source.

To compute the noise generated by 3D flows, the gradient of the Green's function in Eq. (15) should be replaced by[23]

$$\frac{\partial G}{\partial y_i} \approx \frac{\mathrm{i}\omega(x_i - y_i)}{4\pi c_0 R^2} e^{-\frac{\mathrm{i}\omega R}{c_0}}. \tag{17}$$

Equation (17) must satisfy the assumption that the observer is far enough from the sources that the wave number is much greater than the reciprocal of the distance ($\omega/c_0 \gg 1/|\mathbf{x}-\mathbf{y}|$). Terms of $o(1/R)$ are neglected when deriving Eq. (17).

The 3D form of the proposed frequency-domain formulation for the computation of noise generated by the loading term is

$$I_{\mathrm{L}}(\mathbf{x},\omega) = \frac{\mathrm{i}\omega}{4\pi c_0} \int_{-\infty}^{\infty} \int_{f=0} \frac{F_i(x_i - y_i)}{1 + M_R} \frac{1}{R^2} e^{-\mathrm{i}\omega\tau} \mathrm{d}S\mathrm{d}\tau. \tag{18}$$

Note that Eq. (18) is applicable to the far-field sound prediction, and significant error may occur in the case of near-field sound prediction.

3.3. *Details of implementation*

For clarification, we define the integrands in Eqs. (10) and (16) for the noise generated by 2D flows as auxiliary sources as $\tilde{Q}$ and $\tilde{F}$:

$$\tilde{Q}(\mathbf{x},\mathbf{y},\tau) = \frac{Q}{1 + M_R} \left(\frac{1}{R}\right)^{1/2}, \tag{19}$$

$$\tilde{F}(\mathbf{x},\mathbf{y},\tau) = \frac{F_i(y_i - x_i)}{1 + M_R} \left(\frac{1}{R}\right)^{3/2}. \tag{20}$$

By swapping the space and time integrals, the proposed frequency-domain formulation for noise generated by 2D flows then can be rewritten as follows:

$$I_{\mathrm{T}}(\mathbf{x},\omega) = \frac{1}{4} \left(\frac{2\omega c_0}{\pi}\right)^{1/2} e^{\frac{\mathrm{i}\pi}{4}} \int_{f=0} \int_{-\infty}^{\infty} \tilde{Q} e^{-\mathrm{i}\omega\tau} \mathrm{d}\tau\mathrm{d}l, \tag{21}$$

$$I_{\mathrm{L}}(\mathbf{x},\omega) = \frac{-1}{4} \left(\frac{2\omega}{\pi c_0}\right)^{1/2} e^{\frac{\mathrm{i}\pi}{4}} \int_{f=0} \int_{-\infty}^{\infty} \tilde{F} e^{-\mathrm{i}\omega\tau} \mathrm{d}\tau\mathrm{d}l. \tag{22}$$

Note that in an Eulerian frame of reference, the integral boundary $f = 0$ varies with time. We define a coordinate system that is fixed to the moving surface so that $f = 0$ is no longer time-dependent and the space and time integrals can be swapped. We compute the boundary integration by referring to a set of moving points located on the moving boundaries. We track the coordinates of each moving point $\mathbf{Y}(\mathbf{y},t)$ and sample the sources $Q(\mathbf{y},t)$ and $F_i(\mathbf{y},t)$ at the moving points.

Similarly, we can define the integrand in Eqs. (12) and (18) as auxiliary sources $\tilde{Q}$ and $\tilde{F}$ for the noise generated by 3D flows as follows:

$$\tilde{Q}(\mathbf{x},\mathbf{y},\tau) = \frac{Q}{1+M_R}\left(\frac{1}{R}\right), \tag{23}$$

$$\tilde{F}(\mathbf{x},\mathbf{y},\tau) = \frac{F_i(y_i - x_i)}{1+M_R}\left(\frac{1}{R}\right)^2, \tag{24}$$

where $M_R = \frac{1}{c_0}\frac{\mathrm{d}R}{\mathrm{d}t}$ is the Mach number of the source in the direction pointing toward the observer in the 3D flows.

The proposed frequency-domain formulation for noise generated by 3D flows can be rewritten as follows:

$$I_{\mathrm{T}}(\mathbf{x},\omega) = \frac{\mathrm{i}\omega}{4\pi}\int_{f=0}\int_{-\infty}^{\infty}\tilde{Q}e^{-\mathrm{i}\omega\tau}\mathrm{d}\tau\mathrm{dS}, \tag{25}$$

$$I_{\mathrm{L}}(\mathbf{x},\omega) = \frac{-\mathrm{i}\omega}{4\pi c_0}\int_{f=0}\int_{-\infty}^{\infty}\tilde{F}e^{-\mathrm{i}\omega\tau}\mathrm{d}\tau\mathrm{dS}. \tag{26}$$

Usually, it is convenient to sample the variables Q and F_i during a period of $[t_{\mathrm{begin}}, t_{\mathrm{end}}]$ with a constant time step Δt in both numerical simulations and experimental measurements. For periodically oscillating or rotating boundaries, the corresponding variables $\tilde{Q}(\mathbf{x},\mathbf{y},\tau)$ and $\tilde{F}(\mathbf{x},\mathbf{y},\tau)$ given by Eqs. (19) and (20) for 2D flows or Eqs. (23) and (24) for 3D flows in the Fourier transform are not uniformly sampled, because the time intervals between the signals of $\tilde{Q}(\mathbf{x},\mathbf{y},\tau)$ and $\tilde{F}(\mathbf{x},\mathbf{y},\tau)$ depend on both the sampling time step Δt and the velocity of the moving boundary V_i. To use the regular fast Fourier transform (FFT), we must interpolate the variables $\tilde{Q}(\mathbf{x},\mathbf{y},\tau)$ and $\tilde{F}(\mathbf{x},\mathbf{y},\tau)$ to obtain two time series that are uniformly spaced with respect to the new temporal variable with $\Delta\tau \approx \Delta t$. The duration of validity of the uniform time series is $[\tau_{\mathrm{begin,max}}, \tau_{\mathrm{end,min}}]$, where $\tau_{\mathrm{begin,max}}$ is the maximum of τ at the beginning and $\tau_{\mathrm{end,min}}$ is the minimum of τ at the end of motion among all moving boundaries. The detailed procedure for computing the 2D noise using Eqs. (21) and (22) from the sampled thickness and loading sources $Q(\mathbf{y},t)$ and $F_i(\mathbf{y},t)$ can be summarized as follows. It is emphasized that the inputs for the computation are the thickness source $Q(\mathbf{y},t)$ and the loading source $F_i(\mathbf{y},t)$, which are obtained from the velocity and pressure field during the sampling process.

(i) Compute the auxiliary sources $\tilde{Q}(\mathbf{x},\mathbf{y},\tau)$ and $\tilde{F}(\mathbf{x},\mathbf{y},\tau)$ using Eqs. (19) and (20).
(ii) Compute the uniformly spaced time series of auxiliary sources $\tilde{Q}'(\mathbf{x},\mathbf{y},\tau)$ and $\tilde{F}'(\mathbf{x},\mathbf{y},\tau)$ based on the auxiliary sources $\tilde{Q}(\mathbf{x},\mathbf{y},\tau)$ and $\tilde{F}(\mathbf{x},\mathbf{y},\tau)$ with nonuniform time steps by using linear temporal interpolation.
(iii) Transform the uniformly spaced time series of auxiliary sources $\tilde{Q}'(\mathbf{x},\mathbf{y},\tau)$ and $\tilde{F}'(\mathbf{x},\mathbf{y},\tau)$ to the frequency domain using the FFT.
(iv) Calculate the spatial integral on the surface of the moving sources to obtain $I_{\mathrm{T}}(\mathbf{x},\omega)$ and $I_{\mathrm{L}}(\mathbf{x},\omega)$.

The procedure for computing 3D noise can be obtained by replacing Eqs. (19)–(22) with Eqs. (23)–(26), respectively.

We use linear interpolation in step (ii) to obtain the uniformly spaced time series for the regular FFT algorithm. Recall that the interpolation may produce spurious modes in the frequency domain, though these are not encountered in the problems investigated in this work. Steps (ii) and (iii) can be replaced by a NUFFT algorithm to reduce the risk of introducing spurious modes, such as used by Fessler and Sutton[26] where the min-max scaling factor optimization interpolation method is used to minimize the worst-case approximation error over all signals.

Specifically, when the velocity of the moving sources is zero, we have $\frac{1}{1+M_R} = 1$ and $\mathrm{d}\tau = \mathrm{d}t$. Thus, the proposed 2D frequency-domain formulations for the thickness and loading terms reduce to

$$I_{\mathrm{T}}(\mathbf{x},\omega) = \int_{-\infty}^{\infty}\int_{f=0} Q\left(\frac{1}{R}\right)^{1/2}\frac{1}{4}\left(\frac{2\omega c_0}{\pi}\right)^{1/2} e^{\frac{\mathrm{i}\pi}{4}-\frac{\mathrm{i}\omega R}{c_0}} e^{-\mathrm{i}\omega t}\mathrm{d}l\mathrm{d}t, \tag{27}$$

$$I_{\mathrm{L}}(\mathbf{x},\omega) = \int_{-\infty}^{\infty}\int_{f=0} F_i\left(\frac{-(y_i-x_i)}{4}\left(\frac{2\omega}{\pi c_0}\right)^{1/2}\left(\frac{1}{R}\right)^{3/2} e^{\frac{\mathrm{i}\pi}{4}-\frac{\mathrm{i}\omega R}{c_0}}\right) \times e^{-\mathrm{i}\omega t}\mathrm{d}l\mathrm{d}t. \tag{28}$$

The proposed 3D frequency-domain formulations for the thickness and loading terms reduce to

$$I_{\mathrm{T}}(\mathbf{x},\omega) = \int_{-\infty}^{\infty}\int_{f=0} Q\frac{\mathrm{i}\omega}{4\pi R} e^{-\frac{\mathrm{i}\omega R}{c_0}} e^{-\mathrm{i}\omega t}\mathrm{d}S\mathrm{d}t, \tag{29}$$

$$I_{\mathrm{L}}(\mathbf{x},\omega) = \int_{-\infty}^{\infty}\int_{f=0} F_i\left(\frac{(x_i-y_i)}{4\pi}\left(\frac{1}{R}\right)^2 e^{-\frac{\mathrm{i}\omega R}{c_0}}\right) e^{-\mathrm{i}\omega t}\mathrm{d}S\mathrm{d}t. \tag{30}$$

Considering the far-field asymptotic form of the Green's function and its derivation, the thickness and loading terms can be further reduced to

$$I_{\mathrm{T}}(\mathbf{x},\omega) = \int_{f=0} \mathrm{i}\omega\mathcal{F}(Q)G\mathrm{d}l, \tag{31}$$

$$I_{\mathrm{L}}(\mathbf{x},\omega) = \int_{f=0} \mathcal{F}(F_i)\frac{\partial G}{\partial y_i}\mathrm{d}l, \tag{32}$$

which is consistent with the frequency-domain formulation used for the FW-H equation with fixed boundaries.[10]

4. Results and Discussion

First, we validate the accuracy of the proposed frequency-domain formulation by comparing the computed far-field acoustic pressure generated from composite monopoles with the analytical result. Then, we discuss the efficiency of the proposed formulation in computing

the multi-frequency noise generated by composite monopoles and a flapping rectangular wing. Finally, the effects of the rotation velocity on the validity of the formulation and sample frequency requirements are discussed.

4.1. *Multi-frequency noise generated from monopoles with different frequencies*

We validate the proposed frequency-domain formulation by computing the aerodynamic noise generated from composite monopoles fixed in a free space. The ambient medium is at rest. A permeable boundary around the monopole is used to represent a rotating boundary. The velocity potential corresponding to an unsteady monopole is given by[10]

$$\phi(y_1, y_2, t) = \frac{A\mathrm{i}}{4} e^{\mathrm{i}\omega_0 t} H_0^{(2)} \left(\frac{\omega_0}{c_0} \sqrt{y_1^2 + y_2^2} \right), \tag{33}$$

where $H_0^{(2)}$ is the zeroth-order Hankel function of the second kind. A and ω_0 are the amplitude and frequency of the monopole velocity potential, respectively. The composite monopoles consist of 800 unsteady monopoles with different locations and frequencies. The ith monopole is located at $(0.01\cos(2\pi i/800)\,\mathrm{m}, 0.01\sin(2\pi i/800)\,\mathrm{m})$, and the amplitude and frequency of the potential velocity are $(2\pi i/800)^{-0.75}\,\mathrm{m}^2/\mathrm{s}$ and $(0.025\pi i)\mathrm{rad}/s$, respectively. The periods of these monopoles range from 0.1 to 10 s, providing a multi-frequency signal of pressure fluctuations. The pressure, density and velocity fluctuations are the real parts of the following functions:

$$\begin{aligned} p' &= -\rho_0 \frac{\partial \phi}{\partial t}, \\ \rho' &= p'/c_0^2, \\ u_i' &= \frac{\partial \phi}{\partial y_i}, \end{aligned} \tag{34}$$

where ρ_0 and c_0 are equal to $1\,\mathrm{kg/m^3}$ and 340 m/s, respectively. The reference pressure is taken as p_0 in the undisturbed medium. The permeable boundary of the FW-H equation is taken as a square that initially extends from -5 m to 5 m in the y_1 and y_2 directions, respectively. The permeable square rotates around the monopole with an angular velocity of $\omega_{\mathrm{spin}} = 5\pi\,\mathrm{rad}/s$, as shown in Fig. 1.

We uniformly discretize the permeable boundary with a grid length of $L/100$, where L is the edge length of the permeable square. We track the positions $\mathbf{Y}(\mathbf{y}, t)$ at each discretized point and sample $Q(\mathbf{y}, t)$, $F_i(\mathbf{y}, t)$ on the discretized points over a time span of 160 s at time steps of (160/16 384)s.

The acoustic pressure predicted in the frequency domain by the proposed formulation is given in Fig. 2, where the observer position is at $(0\,\mathrm{m}, 1500\,\mathrm{m})$. The pressure spectrum agrees well with the analytical solution especially for comparatively small potential velocity frequencies. The maximum error is less than 2%, corresponding to a frequency of 10 Hz. This

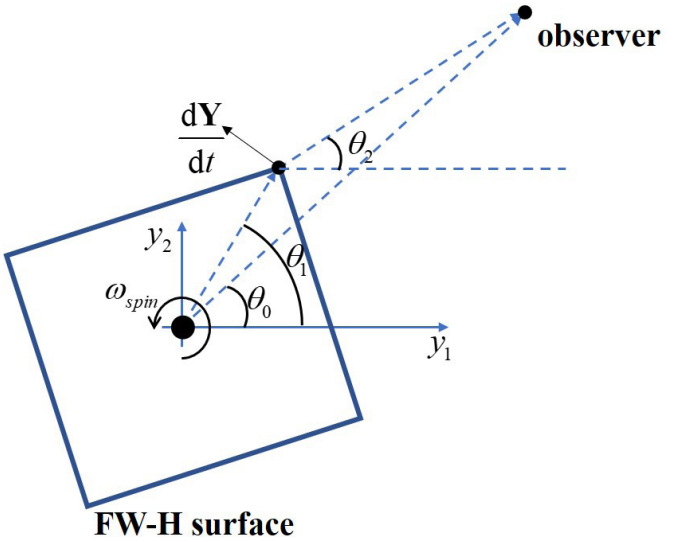

Fig. 1. Schematic of the monopole with a rotating FW-H surface.

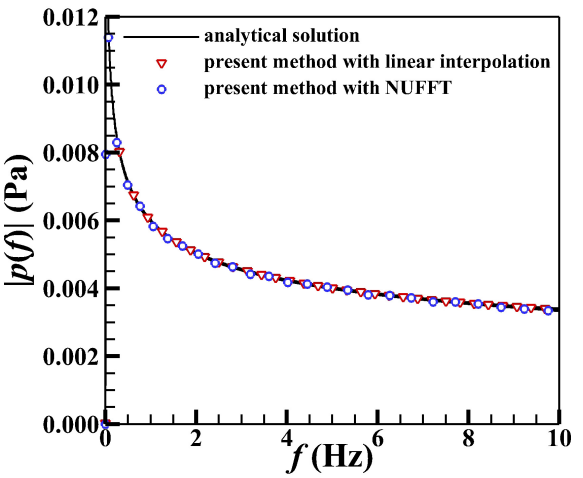

Fig. 2. Pressure spectrum of the multi-frequency noise generated by monopole sources with different frequencies.

indicates that the proposed formulation has the capacity to predict the multi-frequency noise radiated from monopoles at different frequencies.

We also computed the acoustic pressure using the proposed method by replacing steps (ii) and (iii) in Sec. 3.3 with a nonuniform FFT (NUFFT) algorithm. The results are consistent with the analytical solution, with a maximum error of ≈1% in the high frequency region, as shown in Fig. 2. The NUFFT algorithm may use optimized interpolation to reduce the error associated with the interpolation process. This provides an alternative means of

Table 1. Comparison of the number of flops required for the formulation proposed in this work (Eqs. (21) and (22)) and a formulation for tonal noise (Eqs. (6) and (14)).

Name	Symbol	Formulation proposed in this work	Formulation for tonal noise (Eqs. (6) and (14))
Number of Lagrangian points on the moving boundary	N_{L}	400	400
Sampled time span	T_{s}	160 s	160 s
Sampling frequency	f_{s}	(16 384/160) Hz	(16 384/160) Hz
Number of points in sampled time series	N_{P}	16 384	16 384
Number of required Fourier transform or time integration	N_{F}	$N_{\mathrm{F1}} = 1$	$N_{\mathrm{F2}} = 800$
Required flops in computing $I_{\mathrm{T}} + I_{\mathrm{L}}$ at each Lagrangian point	$N_{\mathrm{FT}} + N_{\mathrm{FL}}$	$N_{\mathrm{FT1}} + N_{\mathrm{FL1}}$ $= 2\,293\,760 \approx 2.29 \times 10^6$	$N_{\mathrm{FT2}} + N_{\mathrm{FL2}}$ $= 52\,428\,800 \approx 5.24 \times 10^7$
Required flops in interpolation at each Lagrangian point	N_{FI}	$N_{\mathrm{FI1}} = 147\,456$	$N_{\mathrm{FI2}} = 0$
Required flops in computing the retarded time at each Lagrangian point	N_R	$N_{\mathrm{R1}} = 344\,064 \approx 3.44 \times 10^5$	$N_{\mathrm{R2}} = 344\,064 \approx 3.44 \times 10^5$
Required flops in computing boundary integrals at each Lagrangian point	N_{IN}	$N_{\mathrm{IN1}} = 3200$	$N_{\mathrm{IN2}} = 3200$
Total number of required flops	N_{T}	$N_{\mathrm{T1}} = 1\,115\,392\,000$ $\approx 1.12 \times 10^9$	$N_{\mathrm{T2}} = 21\,110\,425\,600$ $\approx 2.11 \times 10^{10}$
Speedup	S	$N_{\mathrm{T2}}/N_{\mathrm{T1}} \approx 18.9$	

avoiding the explicit interpolation in step (ii) of Sec. 3.3 and improve the results at high frequencies.

We evaluated the efficiency of the proposed method in computing multi-frequency noise in the case where $N_{\mathrm{M}} = 800$ specified frequencies are explicitly provided. Table 1 presents a detailed comparison between the proposed formulation and the conventional frequency-domain formulation for tonal noise (Eqs. (6) and (14)). In this case, the number of discretized Lagrangian grid points on the rotating boundary is $N_{\mathrm{L}} = 400$. We sample the signals at each Lagrangian grid point during a time span of $T_{\mathrm{s}} = 160$ s with a sampling frequency of $f_{\mathrm{s}} = (16\,384/160)$ Hz. The number of points in the time series at each Lagrangian point is $N_{\mathrm{P}} = T_{\mathrm{s}} f_{\mathrm{s}} = 16\,384$.

Using the frequency-domain formulation proposed in this work, we need only to compute the Fourier transforms of I_{T} (Eq. (21)) and I_{L} (Eq. (22)) once ($N_{\mathrm{F}} = 1$) at each Lagrangian point to predict the multi-frequency noise. According to the widely used "radix-2" algorithm

for the FFT,[27] the required number of "flops" (floating-point operations)[28] required to compute the thickness term I_{T} and the loading term I_{L} is given by

$$N_{\mathrm{FT1}} = N_{\mathrm{FL1}} = 5N_{\mathrm{P}}\log_2 N_{\mathrm{P}} = 1\,146\,880 \approx 1.15 \times 10^6. \tag{35}$$

A detailed analysis of the number of flops required in each step can be found in Appendix A. The subscript "1" indicates the first formulation (i.e. the formulation proposed in this work) in Table 1.

The linear interpolation of step (ii) in Sec. 3.3 requires $9N_{\mathrm{P}}$ flops at each Lagrangian point. The number of flops required at each Lagrangian point in computing the retarded time and corresponding variables $\tilde{Q}$ and $\tilde{F}$ in step (i) of Sec. 3.3 is

$$N_{\mathrm{R1}} = (5N_{\mathrm{D}} + 11)N_{\mathrm{P}} = 344\,064 \approx 3.44 \times 10^5, \tag{36}$$

where $N_{\mathrm{D}} = 2$ for 2D problems. The computation of the boundary integral in step (iv) requires $N_{\mathrm{IN1}} = 4N_{\mathrm{M}}$ flops at each Lagrangian point, where $N_{\mathrm{M}} = 800$ is the number of specified frequencies in this case. The total number of flops required in computing the multi-frequency noise is

$$N_{\mathrm{T1}} = N_{\mathrm{L}}(N_{\mathrm{FT1}} + N_{\mathrm{FL1}} + N_{\mathrm{FI1}} + N_{\mathrm{R1}} + N_{\mathrm{IN1}}) \approx 1.12 \times 10^9. \tag{37}$$

By using the conventional frequency-domain formulation for tonal noise (such as Eqs. (6) and (14)), the theoretical number of flops required is $2N_{\mathrm{P}}(N_{\mathrm{P}} - 1)$. According to Cooley and Tukey,[29] the direct use of the discretized Fourier transform (Eqs. (6) and (14)) includes one complex multiplication and one complex addition for each frequency at each Lagrangian point. For the special case investigated in this section, the number of flops can be reduced to $2N_{\mathrm{F}}N_{\mathrm{P}}$, because the N_{F} frequencies have been explicitly given and we only need to compute the integrals in Eqs. (6) and (14) at the N_{F} given frequencies. The number of flops required to compute the thickness and loading terms is

$$N_{\mathrm{FT2}} = N_{\mathrm{FL2}} = 2N_{\mathrm{F}}N_{\mathrm{P}} = 26\,214\,400 \approx 2.62 \times 10^7. \tag{38}$$

The subscript "2" indicates the second formulation (i.e. the formulation for tonal noise) in Table 1. The number of flops required for interpolation at each Lagrangian point is zero, because the linear interpolation is not needed when using Eqs. (6) and (14). However, the computation of the retarded time and the corresponding variables $\tilde{Q}$ and $\tilde{F}$ must still be computed, requiring $N_{\mathrm{R2}} = (5N_{\mathrm{D}} + 11)N_{\mathrm{P}} = 344\,064$ at each Lagrangian point. The computation of the boundary integral requires $N_{\mathrm{IN2}} = 4N_{\mathrm{M}}$ flops at each Lagrangian point. The total number of flops required in computing the multi-frequency noise is

$$N_{\mathrm{T2}} = N_{\mathrm{L}}(N_{\mathrm{FT2}} + N_{\mathrm{FL2}} + N_{\mathrm{FI2}} + N_{\mathrm{R2}} + N_{\mathrm{IN2}}) \approx 2.11 \times 10^{10}. \tag{39}$$

The speedup of the proposed formulation is $S = N_{\mathrm{T2}}/N_{\mathrm{T1}} \approx 18.9$ for this case. This result shows that the proposed formulation is more efficient than the conventional formulation for tonal noise (Eqs. (6) and (14)) in computing the multi-frequency noise generated by composite monopoles.

There are various of frequency-domain formulations for computing tonal noise. The conventional formulation for tonal noise (Eqs. (6) and (14)) investigated in Table 1 might not be the most efficient for multi-frequency noise. However, the trends reported in Table 1 in terms of number of fops are correct. Based on Eqs. (37) and (39), the speedup of the proposed formulation for predicting multi-frequency noise when the frequencies are explicitly given can be expressed as follows:

$$S_E = \frac{N_{\mathrm{L}}(N_{\mathrm{FT2}} + N_{\mathrm{FL2}} + N_{\mathrm{FI2}} + N_{\mathrm{R2}} + N_{\mathrm{IN2}})}{N_{\mathrm{L}}(N_{\mathrm{FT1}} + N_{\mathrm{FL1}} + N_{\mathrm{FI1}} + N_{\mathrm{R1}} + N_{\mathrm{IN1}})} \approx \frac{N_{\mathrm{F}}}{5\log_2 N_{\mathrm{P}}}, \tag{40}$$

where we use the condition that fewer flops are required for linear interpolation and computing retarded time than for FFT. The proposed formulation is efficient when the number of specific frequencies is large ($N_{\mathrm{F}} > 5\log_2 N_{\mathrm{P}}$). This might not be typical for problems with explicitly specified multi-frequencies. However, it can be useful in quickly estimating the features of broadband noise. Equation (40) indicates that the frequency-domain formulation for tonal noise (such as Eqs. (6) and (14)) requires more flops as the number of frequencies (N_{F}) increases. This result is consistent with the discussion of Ghorbaniasl *et al.*,[16] who state that the frequency-domain formulation for tonal noise is computationally expensive when a wide range of frequencies is to be computed.

4.2. *Sound generated by flows around a flapping rectangular wing*

We now compute the noise generated by flows around a benchmark flapping rectangular wing to investigate the efficiency of the 3D frequency-domain formulation proposed in this work. The flapping wing consists of a rectangular flat plate with an aspect ratio of $l_s/l_{\mathrm{c}} = 4.0$, where l_s is the span length and l_{c} the chord length. The flat plate heaves and pitches in a uniform freestream flow in the wind-tunnel frame of reference, as shown in Fig. 3, where the y_1-direction is parallel to the streamwise direction, the y_2-direction is parallel to the spanwise direction, and the y_3-direction is parallel to the vertical direction. The initial center of the rectangular wing (at $t = 0$) is at the origin of the frame of reference. The

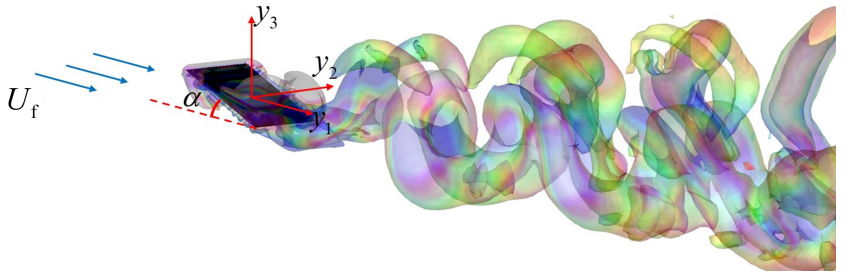

Fig. 3. Schematics of the coordinate system for the flapping rectangular wing.

kinematics of the heaving and pitching are

$$\alpha(t) = \alpha_0 + \alpha_{\mathrm{m}} \cos(2\pi f_0 t),$$
$$y_{3\mathrm{c}}(t) = y_{30} + A \sin(2\pi f_0 t), \tag{41}$$

where $\alpha(t)$ and α_0 are the instantaneous and time-averaged angles of attack, respectively, and α_{m} is the pitching amplitude. $y_{3\mathrm{c}}(t)$ and y_{30} are the instantaneous and time-averaged vertical center positions of the plate, respectively. A is the heaving amplitude and f_0 is the pitching and heaving frequency. These parameters are set, according to the work of Wang *et al.*,[30] as $\alpha_0 = 10°$, $\alpha_{\mathrm{m}} = 30°$, $z_{c0} = 0, A = 0.25\ l_{\mathrm{c}}$ and $f_0 = U_{\mathrm{f}}/l_{\mathrm{c}}$. The freestream velocity U_{f} is 1 m/s and the speed of sound is 340 m/s. The Reynolds number and the Mach number based on the freestream velocity are 300 and 1/340, respectively. More details of the flows and forces can be found in our previous work.[30–32]

We computed the noise at the far-field using the proposed formulation (Eqs. (25) and (26)) and the conventional frequency-domain formulation for tonal noise (Eqs. (6) and (14)). The Green's function for the medium at rest is used to approximate the Green's function for the convective wave equation considering that the Doppler effect is weak at the low Mach number investigated in this case. The sound pressure spectrum predicted by the proposed formulation is consistent with that predicted by the formulation for tonal noise (Eqs. (6) and (14)), as shown in Fig. 4.

Table 2 presents a detailed comparison of the proposed formulation and the conventional frequency-domain formulation for tonal noise (Eqs. (6) and (14)). In this case, the number of discretized Lagrangian grid points on the flapping rectangular flat plate is $N_{\mathrm{L}} = 10\,000$. We sample the signals at each Lagrangian grid point over a time span of $T_{\mathrm{s}} = 15U_{\mathrm{f}}/l_{\mathrm{c}}$ with a sampling frequency of $f_{\mathrm{s}} = 200U_{\mathrm{f}}/l_{\mathrm{c}}$. The number of points in the time series of the signals at each Lagrangian point is $N_{\mathrm{P}} = T_{\mathrm{s}} f_{\mathrm{s}} = 3000$.

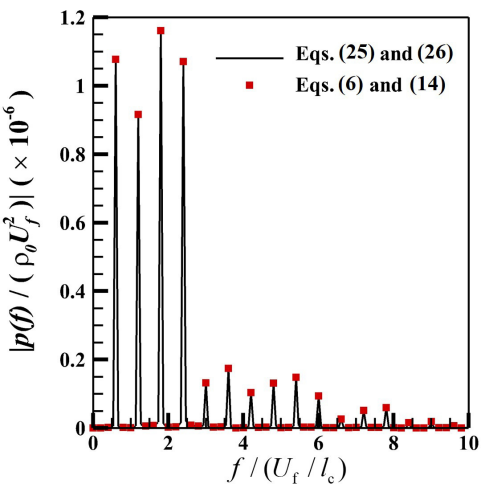

Fig. 4. Pressure spectrum of acoustic pressure generated by flapping flight using different formulations.

Table 2. Comparison of the prediction of sound generated by flows around a flapping rectangular wing between using Eqs. (25) and (26) or using Eqs. (6) and (14).

Name	Symbol	Formulation proposed in this work	Formulation for tonal noise (Eqs. (6) and (14))
Number of Lagrangian points on the moving boundary	N_{L}	10 000	10 000
Sampled time span	T_{s}	$15U_{\mathrm{f}}/l_{\mathrm{c}}$	$15U_{\mathrm{f}}/l_{\mathrm{c}}$
Sampling frequency	f_{s}	$200U_{\mathrm{f}}/l_{\mathrm{c}}$	$200U_{\mathrm{f}}/l_{\mathrm{c}}$Hz
Number of points in sampled time series	N_{P}	3000	3000
Number of required Fourier transform or time integration	N_{F}	1	2999
Required flops in computing $I_{\mathrm{T}} + I_{\mathrm{L}}$ at each Lagrangian point	$N_{\mathrm{FT}} + N_{\mathrm{FL}}$	$N_{\mathrm{FT1}} + N_{\mathrm{FL1}}$ $= 491\,520 \approx 4.92 \times 10^5$	$N_{\mathrm{FT2}} + N_{\mathrm{FL2}}$ $= 35\,988\,000 \approx 3.60 \times 10^7$
Required flops in interpolation at each Lagrangian point	N_{FI}	$N_{\mathrm{FI1}} = 27\,000$	$N_{\mathrm{FI2}} = 0$
Required flops in computing the retarded time at each Lagrangian point	N_R	$N_{\mathrm{R1}} \approx 7.5 \times 10^4$	$N_{\mathrm{R2}} \approx 7.5 \times 10^4$
Required flops in computing boundary integrals at each Lagrangian point	N_{IN}	$N_{\mathrm{IN1}} = 12\,000$	$N_{\mathrm{IN2}} = 12\,000$
Total number of required flops	N_{T}	$N_{\mathrm{T1}} = 6\,055\,200\,000$ $\approx 6.06 \times 10^9$	$N_{\mathrm{T2}} = 360\,750\,000\,000$ $\approx 3.61 \times 10^{11}$
Speedup	S	$N_{\mathrm{T2}}/N_{\mathrm{T1}} \approx 59.6$	

As discussed in Sec. 4.3, the Fourier transforms of I_{T} (Eq. (25)) and I_{L} (Eq. (26)) are computed only once ($N_{\mathrm{F}} = 1$) at each Lagrangian point in predicting the multi-frequency noise using the frequency-domain formulation proposed in this work. The number of flops required for computing the thickness term I_{T} and the loading term I_{L} is

$$N_{\mathrm{FT1}} = N_{\mathrm{FL1}} = 5N_{\mathrm{P}'}\log_2 N_{\mathrm{P}'} = 245\,760 \approx 2.46 \times 10^5. \tag{42}$$

In the original time series, $N_{\mathrm{P}} = 3000$, which is unsuitable for the FFT. The original time series needs to be extended to 2^{n_1} points.[27] The expanded time series of signals at each Lagrangian point on the flapping rectangular wing consists of $N'_{\mathrm{P}} = 4096 = 2^{12}$. The subscript "1" indicates the first formulation (i.e. the formulation proposed in this work) in Table 2. The number of flops required for linear interpolation at each Lagrangian point is $N_{\mathrm{FI1}} = 27\,000$. The number of flops required to compute the retarded time and the variables $\tilde{Q}$ and $\tilde{F}$ in step (i) of Sec. 3.3 is $N_{\mathrm{R1}} = (5N_{\mathrm{D}} + 10)N_{\mathrm{P}} \approx 7.5 \times 10^4$, where $N_{\mathrm{D}} = 3$ for

3D flows. The computation of the surface integral in step (iv) requires $N_{\mathrm{IN1}} = 4N_{\mathrm{P}}$ flops at each Lagrangian point. The total number of flops required in computing the multi-frequency noise is

$$N_{\mathrm{T1}} = N_{\mathrm{L}}(N_{\mathrm{FT1}} + N_{\mathrm{FL1}} + N_{\mathrm{FI1}} + N_{\mathrm{R1}} + N_{\mathrm{IN1}}) \approx 6.06 \times 10^9. \tag{43}$$

Unlike the case in Sec. 4.3, where the frequencies of the noise were known, the frequency ω is not known in this case before we conduct the Fourier transform. According to the work of Cooley and Tukey,[29] the direct use of the discretized Fourier transform (Eqs. (6) and (14)) includes one complex multiplication and one complex addition for each frequency at each Lagrangian point. Thus, the number of required flops is $2N_{\mathrm{P}}(N_{\mathrm{P}} - 1)$ when the frequency-domain formulation for tonal noise (Eqs. (6) and (14)) is employed to compute the multiple-frequency noise,

$$N_{\mathrm{FT2}} = N_{\mathrm{FL2}} = 2N_{\mathrm{P}}(N_{\mathrm{P}} - 1) = 17\,994\,000 \approx 1.80 \times 10^7. \tag{44}$$

The subscript "2" indicates the second formulation (i.e. the formulation for tonal noise) in Table 2. The number of flops required for the interpolation at each Lagrangian point is zero, because the linear interpolation is not needed when using Eqs. (6) and (14). The computations of the retarded time and the corresponding variables $\tilde{Q}$ and $\tilde{F}$ are still necessary, requiring $N_{\mathrm{R2}} = (5N_{\mathrm{D}} + 10)N_{\mathrm{P}} = 75\ 000$ flops at each Lagrangian point. In addition, the surface integral computation requires $N_{\mathrm{IN2}} = 4N_{\mathrm{P}}$ flops at each Lagrangian point. The total number of flops required in computing the noise using the formulation for tonal noise is

$$N_{\mathrm{T2}} = N_{\mathrm{L}}(N_{\mathrm{FT2}} + N_{\mathrm{FL2}} + N_{\mathrm{FI2}} + N_{\mathrm{R2}} + N_{\mathrm{IN2}}) \approx 3.61 \times 10^{11}. \tag{45}$$

The speedup of the proposed formulation is $S = N_{\mathrm{T2}}/N_{\mathrm{T1}} \approx 59.6$ for this case. This result shows that the proposed formulation is more efficient than the conventional formulation for tonal noise (Eqs. (6) and (14)).

As discussed in Sec. 4.3, the formulation for tonal noise (Eqs. (6) and (14)) investigated in Table 2 might not be the most efficient for computing multi-frequency noise generated by flapping wings. However, the trends in the number of flops reported in Table 2 should be correct. From Eqs. (43) and (45), the speedup of the proposed formulation for predicting multi-frequency noise without explicitly given frequencies can be expressed as follows:

$$\begin{aligned} S_{\mathrm{I}} &= \frac{N_{\mathrm{L}}(N_{\mathrm{FT2}} + N_{\mathrm{FL2}} + N_{\mathrm{FI2}} + N_{\mathrm{R2}} + N_{\mathrm{IN2}})}{N_{\mathrm{L}}(N_{\mathrm{FT1}} + N_{\mathrm{FL1}} + N_{\mathrm{FI1}} + N_{\mathrm{R1}} + N_{\mathrm{IN1}})} \\ &\approx \frac{N_{\mathrm{P}}}{5\log_2 N_{\mathrm{P}}}. \end{aligned} \tag{46}$$

It is assumed that fewer flops are required for linear interpolation and computing the retarded time than for the FFT. The proposed formulation is efficient when the number of points in the sampled time series satisfies $N_{\mathrm{P}} > 5\log_2 N_{\mathrm{P}}$.

We also compared the CPU time and wall-clock time required by the different formulations. Here, the CPU time and wall-clock time are defined according to the work of

Pacheco.[33] The CPU time is defined as the amount of time that the CPU spends in processing the instructions of a program. The wall-clock time is defined as the amount of time that the program takes from start to finish. The computation of noise was conducted on a workstation powered by a 2.93 GHz Intel Xeon X5670 processor and 24 GB DDR3 memory. The computations reported in Fig. 4 using the proposed formulation required 280.9 s CPU time and 735.3 s wall-clock time, while the conventional frequency-domain formulation (Eqs. (6) and (14)) required 7726.8 s CPU time and 8469.6 s wall-clock time, respectively. The speedups factors of the proposed formulation are 27.5 in terms of CPU time and 11.5 in terms of wall-clock time, listed in Table 3. The speedup factors obtained from the flops, CPU time and wall-clock time are different. This is because they reflect different aspects of efficiency. The measurement of flops reflects the required floating-point operations but does not distinguish between addition and multiplication operations. The CPU time reflects the total time of processing the required flops, but does not account for the I/O or system operation times. That is, the CPU time is highly-dependent on the computer hardware. For example, the use of a coprocessor in a field-programmable gate array can significantly reduce the CPU time for floating-point operations. The wall-clock time counts all of the time required to run code. The wall-clock time may depend on both the hardware and software of the computer. However, the comparisons of flops, CPU time and wall-clock time show that the proposed formulation is more efficient than the conventional frequency-domain formulation.

4.3. *Constraints on the rotation velocity*

One constraint of the proposed method is that the freestream Mach number must approach 0, because we have neglected the effects of convection on the far-field sound radiation. Furthermore, to avoid a singularity in the integral function, the proposed method should be limited to sound prediction of FW-H surfaces in subsonic motion. A detailed derivation is presented in this section.

We have introduced a new temporal variable $\tau = t + R/c_0$, which results in $\mathrm{d}t = \frac{\mathrm{d}\tau}{1+M_R}$ with $M_R = \frac{1}{c_0}\frac{\mathrm{d}R}{\mathrm{d}t}$ being the Mach number defined by the velocity of the moving source $\frac{\mathrm{d}R}{\mathrm{d}t}$ and the speed of sound c_0. In the computation of the acoustic pressure with the proposed formulation, we need to avoid a rotation velocity that causes $1 + M_R = 0$; i.e. we need to ensure that $1 + M_R \neq 0$ when applying the proposed formulation.

Table 3. CPU time and wall-clock time comparison of serial computations for one observer from 3000 temporal samples with 10 000 grid points. Computations were performed on a 2.93 GHz, Intel Xeon X5670.

	Formulation proposed in this work	Formulation for tonal noise (Eqs. (6) and (14))	Speedup
CPU time	280.9 s	7726.8 s	27.5
Wall-clock time	735.3 s	8469.6 s	11.5

Note that R is $\sqrt{(Y_1 - x_1)^2 + (Y_2 - x_2)^2}$ for 2D problems. Thus, we have

$$\begin{aligned} M_R &= \frac{1}{c_0}\frac{\mathrm{d}R}{\mathrm{d}t} \\ &= \frac{1}{c_0}\frac{\mathrm{d}\sqrt{(Y_1 - x_1)^2 + (Y_2 - x_2)^2}}{\mathrm{d}t} \\ &= \frac{1}{c_0}\frac{\left((Y_1 - x_1)\frac{\mathrm{d}(Y_1 - x_1)}{\mathrm{d}t} + (Y_2 - x_2)\frac{\mathrm{d}(Y_2 - x_2)}{\mathrm{d}t}\right)}{\sqrt{(Y_1 - x_1)^2 + (Y_2 - x_2)^2}} \\ &= \frac{1}{c_0}\left(\frac{(Y_1 - x_1)}{R}\frac{\mathrm{d}(Y_1 - x_1)}{\mathrm{d}t} + \frac{(Y_2 - x_2)}{R}\frac{\mathrm{d}(Y_2 - x_2)}{\mathrm{d}t}\right). \end{aligned} \tag{47}$$

According to Fig. 1, $\frac{(Y_1 - x_1)}{R}$ is $-\cos\theta_2$ and $\frac{(Y_2 - x_2)}{R}$ is $-\sin\theta_2$. In addition, $\frac{\mathrm{d}(Y_1 - x_1)}{\mathrm{d}t}$ and $\frac{\mathrm{d}(Y_2 - x_2)}{\mathrm{d}t}$ are equal to $-\left|\frac{\mathrm{d}\mathbf{Y}}{\mathrm{d}t}\right|\sin\theta_1$ and $\left|\frac{\mathrm{d}\mathbf{Y}}{\mathrm{d}t}\right|\cos\theta_1$, respectively. Hence, Eq. (47) can be further reduced to

$$\begin{aligned} M_R &= \frac{1}{c_0}\left(\frac{(Y_1 - x_1)}{R}\frac{\mathrm{d}(Y_1 - x_1)}{\mathrm{d}t} + \frac{(Y_2 - x_2)}{R}\frac{\mathrm{d}(Y_2 - x_2)}{\mathrm{d}t}\right) \\ &= \frac{1}{c_0}(\cos\theta_2\sin\theta_1 - \cos\theta_1\sin\theta_2)\left|\frac{\mathrm{d}\mathbf{Y}}{\mathrm{d}t}\right| \\ &= \frac{\sin(\theta_1 - \theta_2)}{c_0}\left|\frac{\mathrm{d}\mathbf{Y}}{\mathrm{d}t}\right|. \end{aligned} \tag{48}$$

Therefore, for the computation of the far-field acoustic pressure, the inequality $1 + M_R \neq 0$ can be expressed as

$$1 + \frac{\sin(\theta_1 - \theta_2)}{c_0}\left|\frac{\mathrm{d}\mathbf{Y}}{\mathrm{d}t}\right| \neq 0. \tag{49}$$

As the observer position is assumed to be in the far-field, θ_2 is approximately equal to θ_0, as shown in Fig. 1. For each point on the rotating boundary, θ_1 ranges from 0 to 2π. Therefore, $\sin(\theta_1 - \theta_2)$ varies from -1 to 1. The condition $\frac{1}{c_0}\left|\frac{\mathrm{d}\mathbf{Y}}{\mathrm{d}t}\right|_{\max} < 1$ is is necessary to ensure that Eq. (49) holds. For a boundary rotation as a rigid body, the rotating velocity should satisfy $\omega_{\mathrm{spin}} < c_0/l_{\max}$, where $l_{\max}$ is the maximum distance between the boundary and the rotating center. The same constraint can be obtained for the noise generated by 3D flows.

4.4. *Effects of a rotating boundary on the sampling frequency*

To compute the sound pressure, the flow information at the boundary must be sampled with the FW-H equation. For problems with a fixed boundary, the sampling frequency depends on the frequency of the sound, and this has been widely investigated to obtain the correct sound signal. For problems with rotating boundaries, as investigated in this work, the sampling frequency depends on both the frequency of the sound and the rotation velocity of the

boundary. We must therefore consider the sampling frequency when addressing problems with rotating boundaries.

We use the benchmark flow generated by the monopole in Sec. 4.1 to investigate the effects of a rotating boundary on the sampling frequency. The same parameters are used to set up the flows and numerical computations, except for the sampling frequency, unsteady monopole frequency ω_0, and rotating velocity of the permeable square ω_{spin}. To identify the minimum number of sampling points, we fix the sampling time step at $(20/512)$ s and vary the monopole frequency ω_0 and rotation velocity ω_{spin} from 2π rad/s to 14π rad/s. Details of the settings for the monopole frequency ω_0 and rotation velocity ω_{spin} are presented in Table 4.

In cases A–D, the rotation velocity is fixed at $\omega_{\text{spin}} = 2\pi$ rad/s, and the monopole frequencies are set to 2π, 6π, 10π and 14π rad/s, respectively. The sound pressure predicted by the proposed method is shown in Figs. 5(a)–5(d). The results show that the predicted sound pressure matches the analytical expression well as long as the monopole frequency $\omega_0 \leq 10\pi$ rad/s. The sound pressure is overpredicted by 25.4% when the monopole frequency reaches 14π rad/s.

In cases E–H, the monopole frequency is fixed at $\omega_0 = 2\pi$ rad/s, and the rotation velocities are set to 2π, 6π, 10π and 14π rad/s, respectively. The sound pressure predicted by the proposed method for each case is shown in Figs. 5(e)–5(h). The results show that the predicted sound pressure matches the analytical expression well when the rotation velocity

Table 4. Setups for the monopole frequency and rotation velocity of cases A-H.

Cases	A	B	C	D	E	F	G	H
ω_0(rad/s)	2π	6π	10π	14π	2π	2π	2π	2π
ω_{spin}(rad/s)	2π	2π	2π	2π	2π	6π	10π	14π

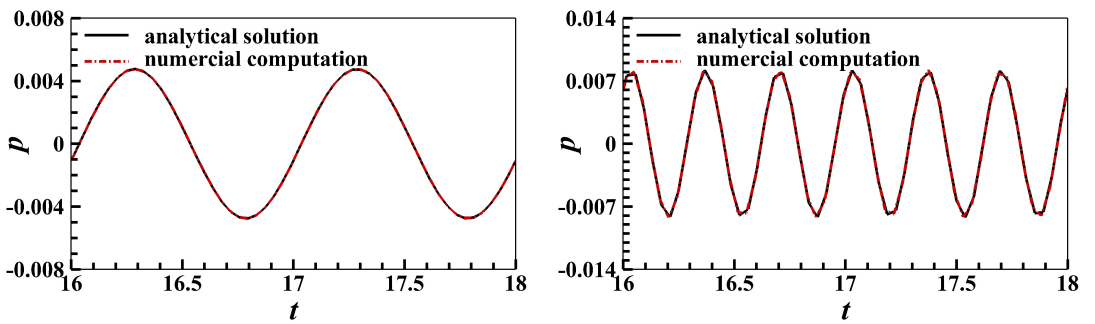

(a) (b)

Fig. 5. Effects of different sampling frequencies on the far-field pressure fluctuations. (a)–(d) correspond to ω_0 values of 2π, 6π, 10π and 14π, respectively; (e)–(h) correspond to ω_{spin} values of 2π, 6π, 10π and 14π rad/s, respectively. p and t in the figure have been nondimensionized by 1 Pa and 1 s, respectively.

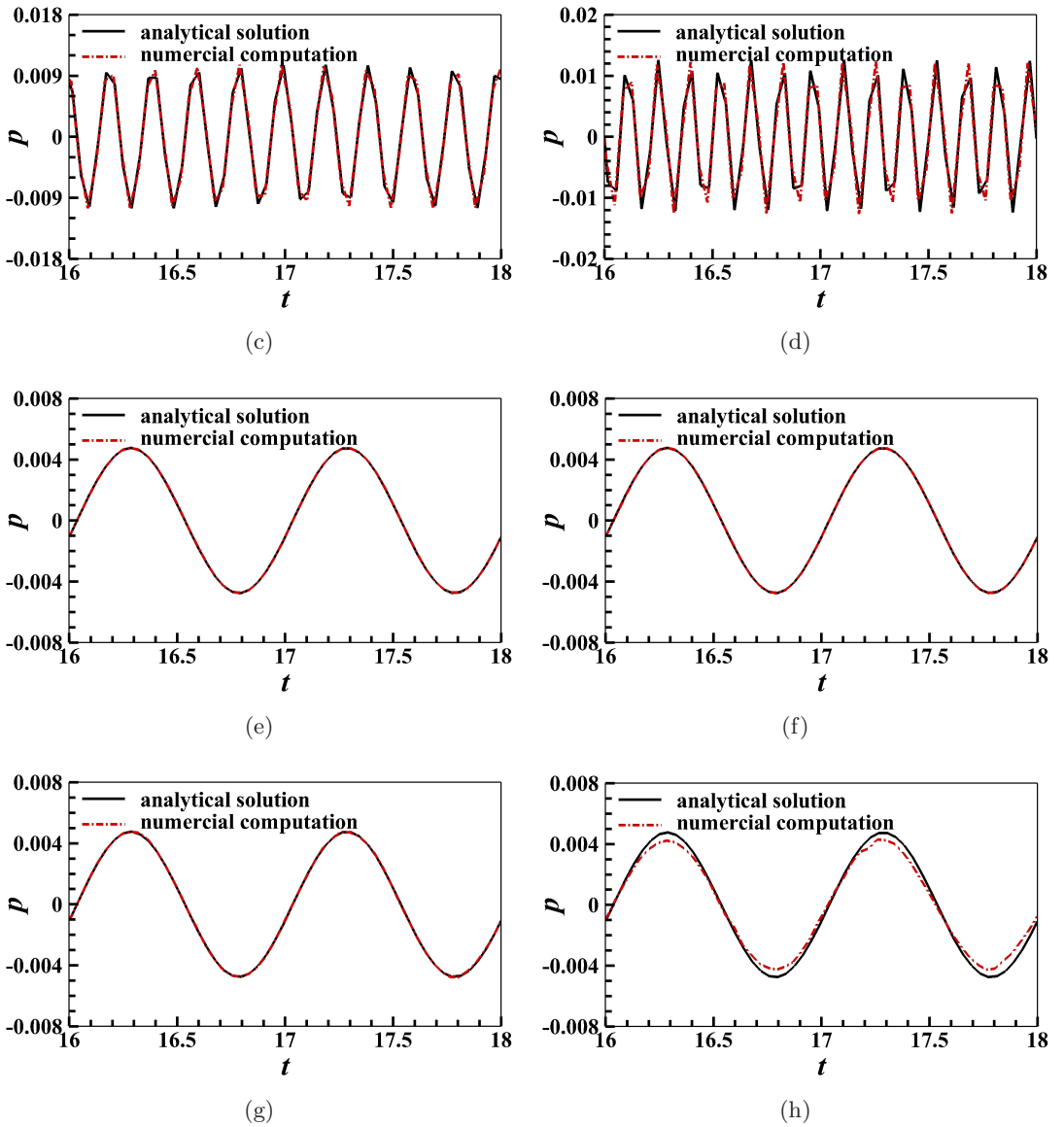

Fig. 5. (*Continued*)

$\omega_{\text{spin}} \leq 10\pi$ rad/s. The sound pressure is underpredicted by 11.5% when the rotation velocity reaches 14π rad/s.

For the cases considered in this section, the sampling time step is fixed at (20/512)s and the sampling time span is 20 s. The predicted sound pressure agrees well with the analytical solution when the sound frequency does not exceed 10π rad/s or the rotation velocity of the boundary does not exceed 10π rad/s. The results indicate that at least approximately, five points must be sampled in each characteristic period T, defined by $T = \min(2\pi/\omega_0, 2\pi/\omega_{\text{spin}})$. The results confirm that the required sampling frequency

depends on both the frequency of the sound and the rotation velocity of the boundary. We have provided a brief estimation of the required sampling frequency for an unsteady monopole with a rotating permeable square boundary. Note that the sampling frequency also depends on the frequency of the flow. The minimum sampling frequency might vary with the flow and the rotating boundaries. A more detailed discussion on the required sampling frequency for complex flows is needed for specific applications, although this is beyond the scope of this work.

5. Conclusions

We have proposed a frequency-domain formulation for computing the far-field noise generated by flows with periodically oscillating or rotating boundaries. The proposed formulation predicts broadband noise or multi-frequency noise at the far-field by efficiently computing the FW-H integrals for the thickness and loading terms. The novelty of this work is that the far-field asymptotic Green's function is used to separate the frequency- and time-dependent components in the FW-H integrals. This significantly simplifies the computation and circumvents the expensive time integration in computing the multi-frequency and broadband noise when using the frequency-domain formulation. The proposed formulation has the advantages of identifying noise at different frequencies by computing the Fourier transform only once. The efficiency of the proposed formulation has been analyzed in detail by comparing the required number of flops with that of a conventional frequency-domain formulation. In predicting the multi-frequency noise with explicitly given frequencies, the efficiency of the proposed method approximately scales with $N_{\mathrm{F}}/(5\log_2 N_{\mathrm{P}})$, where N_{F} is the number of explicitly given frequencies and N_{P} is the number of points in the time series of signals. In predicting the broadband noise without explicitly given frequencies, the efficiency of the proposed method approximately scales with $N_{\mathrm{P}}/(5\log_2 N_{\mathrm{P}})$ when N_{P} is large. We validated the proposed formulation using a flow generated by composite monopoles. The results show that the proposed formulation correctly predicts the time-dependent acoustic pressure. The efficiency of the proposed method was validated by computing the multi-frequency noise generated by composite monopoles and a flapping rectangular wing. To ensure the accuracy of the sound prediction, the proposed method must satisfy certain constraints. The translational speed of the moving boundary should be low enough that the Doppler effect corresponding to the freestream flow can be neglected. The observer should be far enough from the source region. The wave number should be much greater than the reciprocal of the distance between the observer and source. The rotation velocity of a rigid body should satisfy $\omega_{\mathrm{spin}} < c_0/l_{\max}$, where $l_{\max}$ is the maximum distance between the boundary and the rotating center. The sampling frequencies vary with the boundary moving velocity as discussed in Sec. 4.4.

Acknowledgments

This work is supported by the NSFC Basic Science Center Program for "Multiscale Problems in Nonlinear Mechanics" (No. 11988102), the National Natural Science Foundation of

China (Nos. 11922214 and 91952301), Pilot National Laboratory for Marine Science and Technology (Qingdao, Wenhai Project 2021WHZZB1400). The computations are conducted on Tianhe-1 at the National Supercomputer Center in Tianjin.

References

1. Y. Dai, Y. An, Z. Li and Q. Zhang, Numerical simulation of noise generated by shock (wave) and boundary layer interaction in aero-engine inlet, *Acta Mech. Sin.* **38** (2022) 1–11.
2. I. Z. Naqavi, Z.-N. Wang, P. G. Tucker, M. Mahak and P. Strange, Far-field noise prediction for jets using large-eddy simulation and Ffowcs Williams–Hawkings method, *Int. J. Aeroacoust.* **15** (2016) 757–780.
3. F. Mao, L. Kang, L. Liu and J. Wu, A unified theory for gas dynamics and aeroacoustics in viscous compressible flows. Part I. Unbounded fluid, *Acta Mech. Sin.* **38** (2022) 1–15.
4. H.-D. Yao, L. Davidson and L.-E. Eriksson, Noise radiated by low-Reynolds number flows past a hemisphere at Ma = 0.3, *Phys. Fluids* **29** (2017) 076102.
5. C. Chenghua, D. Xiaogang and M. Meiliang, Advances in complex low speed flow around a prolate spheroid, *Adv. Mech.* **51** (2021) 467–619.
6. J. E. Ffowcs Williams and D. L. Hawkings, Sound generation by turbulence and surfaces in arbitrary motion, *Philos. Trans. R. Soc. A* **264** (1969) 321–342.
7. M. J. Lighthill, On sound generated aerodynamically I. General theory, *Philos. Trans. R. Soc. A* **211** (1952) 564–587.
8. F. Farassat and G. P. Succi, A review of propeller discrete frequency noise prediction technology with emphasis on two current methods for time domain calculations, *J. Sound Vib.* **71** (1980) 399–419.
9. A. Najafi-Yazdi, G. A. Brès and L. Mongeau, An acoustic analogy formulation for moving sources in uniformly moving media, *Philos. Trans. R. Soc. A* **467** (2011) 144–165.
10. D. P. Lockard, An efficient, two-dimensional implementation of the Ffowcs Williams and Hawkings equation, *J. Sound Vib.* **229** (2000) 897–911.
11. Y. Guo, Application of the Ffowcs Williams/Hawkings equation to two-dimensional problems, *J. Fluid Mech.* **403** (2000) 201–221.
12. H. Xia, P. G. Tucker and S. Eastwood, Large-eddy simulations of chevron jet flows with noise predictions, *Int. J. Heat Fluid Flow* **30** (2009) 1067–1079.
13. A. Tadamasa and M. Zangeneh, Numerical prediction of wind turbine noise, *Renew. Energy* **36** (2011) 1902–1912.
14. W. Zhu, Z. Xiao and S. Fu, Numerical modeling screen for flow and noise control around tandem cylinders, *AIAA J.* **58**(6) (2020) 2504–2516.
15. K. S. Brentner and F. Farassat, Modeling aerodynamically generated sound of helicopter rotors, *Prog. Aerosp. Sci.* **39** (2003) 83–120.
16. G. Ghorbaniasl, Z. Huang, L. Siozos-Rousoulis and C. Lacor, Analytical acoustic pressure gradient prediction for moving medium problems, *Philos. Trans. R. Soc. A* **471** (2015) 20150342.
17. M. Gennaretti, C. Testa and G. Bernardini, Frequency-domain method for discrete frequency noise prediction of rotors in arbitrary steady motion, *J. Sound Vib.* **331** (2012) 5502–5517.
18. A. Bozorgi, L. Siozos-Rousoulis, S. A. Nourbakhsh and G. Ghorbaniasl, A two-dimensional solution of the FW-H equation for rectilinear motion of sources, *J. Sound Vib.* **388** (2017) 216–229.
19. D. Lockard, A comparison of Ffowcs Williams–Hawkings solvers for airframe noise applications, in *8th AIAA/CEAS Aeroacoustics Conf. and Exhibit* (Breckenridge, US, 2002), p. 2580.
20. F. Farassat, Derivation of Formulations 1 and 1A of Farassat, Technical Report (2007).

21. M. Wang, S. K. Lele and P. Moin, Computation of quadrupole noise using acoustic analogy, *AIAA J.* **34** (1996) 2247–2254.
22. T. Ikeda, S. Enomoto, K. Yamamoto and K. Amemiya, Quadrupole corrections for the permeable-surface Ffowcs Williams–Hawkings equation, *AIAA J.* **55** (2017) 2307–2320.
23. Z. Zhou, H. Wang, S. Wang and G. He, Lighthill stress flux model for Ffowcs Williams–Hawkings integrals in frequency domain, *AIAA J.* **59** (2021) 4809–4814.
24. Z. Zhou, H. Wang and S. Wang, Simplified permeable surface correction for frequency-domain Ffowcs Williams and Hawkings integrals, *Theor. App. Mech. Lett.* **11** (2021) 100259.
25. Z. Zhou, Z. Zang, H. Wang and S. Wang, Far-field approximations to the derivatives of Greens function for the Ffowcs Williams and Hawkings equation, *Adv. Aerodyn.* **4** (2022) 1–23.
26. J. A. Fessler and B. P. Sutton, Nonuniform fast Fourier transforms using min-max interpolation, *IEEE Trans. Signal Process.* **51** (2003) 560–574.
27. M. Frigo and S. G. Johnson, The design and implementation of FFTW3, *Proc. IEEE Inst. Electr. Electron. Eng.* **93** (2005) 216–231.
28. S. G. Johnson and M. Frigo, A modified split-radix FFT with fewer arithmetic operations, *IEEE Trans. Signal Process.* **55** (2006) 111–119.
29. J. W. Cooley and J. W. Tukey, An algorithm for the machine calculation of complex Fourier series, *Math. Comput.* **19** (1965) 297–301.
30. S. Wang, G. He and T. Liu, Estimating lift from wake velocity data in flapping flight, *J. Fluid Mech.* **868** (2019) 501–537.
31. S. Wang, X. Zhang, G. He and T. Liu, Evaluation of lift formulas applied to low-Reynolds-number unsteady flows, *AIAA J.* **53** (2015) 161–175.
32. S. Wang, X. Zhang, G. He and T. Liu, A lift formula applied to low-Reynolds-number unsteady flows, *Phys. Fluids* **25** (2013) 093605.
33. P. Pacheco, *An Introduction to Parallel Programming* (Elsevier, 2011).
34. L. N. Trefethen and D. Bau III, *Numerical Linear Algebra*, Vol. 50 (SIAM, 1997).

Appendix A. Analysis of the Required Number of Floating-point Operations

In this section, we report the details of the estimation of the number of floating-point operations (flops) required by the proposed formulation for 2D noise (Eqs. (21) and (22)) and 3D noise (Eqs. (25) and (26)). The number of flops required by the conventional frequency-domain formulation (Eqs. (6) and (14)) in computing the same problem with multi-frequency or broadband noise are also analyzed. We estimate the number of flops according to the work of Trefethen and Bau[34] where each addition, subtraction, multiplication, division or square root counts as one flop.

Table A.1 presents the required number of flops for the proposed frequency-domain formulation for 2D noise (Eqs. (21) and (22)). Our estimations are based on the setup of N_{L} Lagrangian points on the moving boundary and N_{P} elements in the time series of the signal at each Lagrangian point.

In step (i), for computing the 2D noise at each Lagrangian point and each time step, the computation of the distance $R = \sqrt{(x_1 - y_1)^2 + (x_2 - y_2)^2}$ requires $3N_{\mathrm{D}}$ flops which includes N_{D} subtractions, N_{D} multiplications, $N_{\mathrm{D}} - 1$ additions and one square root. The computation of $\tau = t + R/c_0$ requires two more flops after the distance R has been computed. Therefore, the total number of flops required in computing τ is $3N_{\mathrm{D}} + 2$. The computation of

Table A.1. Flops for the 2D formulation proposed in this work (Eqs. (21) and (22)).

Step order and symbol	Required computation	Number of flops	Total number of flops in each step
Step (i) (N_{R1})	$\tau = t + R/c_0$	$(3N_{\mathrm{D}}+2)N_{\mathrm{L}}N_{\mathrm{P}}$	$(5N_{\mathrm{D}}+11)N_{\mathrm{L}}N_{\mathrm{P}}$
	$\tilde{Q} = \frac{Q}{1+M_R}\left(\frac{1}{R}\right)^{\frac{1}{2}}$	$8N_{\mathrm{L}}N_{\mathrm{P}}$	
	$\tilde{F} = \frac{F_i(y_i-x_i)}{1+M_R}\left(\frac{1}{R}\right)^{\frac{3}{2}}$	$(2N_{\mathrm{D}}+1)N_{\mathrm{L}}N_{\mathrm{P}}$	
Step (ii) (N_{FI1})	$\tilde{Q}'_j = \tilde{Q}_i\lambda_1 + \tilde{Q}_{i+1}(1-\lambda_1)$	$6N_{\mathrm{L}}N_{\mathrm{P}}$	$9N_{\mathrm{L}}N_{\mathrm{P}}$
	$\tilde{F}'_j = \tilde{F}_i\lambda_1 + \tilde{F}_{i+1}(1-\lambda_1)$	$3N_{\mathrm{L}}N_{\mathrm{P}}$	
Step (iii) (N_{FT1}, N_{FL1})	fast Fourier transform of $\tilde{Q}'$	$5N_{\mathrm{L}}N_{\mathrm{P}}\log_2 N_{\mathrm{P}}$	$10N_{\mathrm{L}}N_{\mathrm{P}}\log_2 N_{\mathrm{P}}$
	fast Fourier transform of $\tilde{F}'$	$5N_{\mathrm{L}}N_{\mathrm{P}}\log_2 N_{\mathrm{P}}$	
Step (iv) (N_{IT1}, N_{IL1})	boundary integration of $\mathcal{F}(\tilde{Q}')$	$2N_{\mathrm{L}}N_{\mathrm{P}}$	$4N_{\mathrm{L}}N_{\mathrm{P}}$
	boundary integration of $\mathcal{F}(\tilde{F}')$	$2N_{\mathrm{L}}N_{\mathrm{P}}$	

the Mach number M_R requires three more flops, including one subtraction and two divisions. With the computed Mach number M_R, the computation of the auxiliary thickness source $\tilde{Q}$ requires five more flops, including one addition, one multiplication, one square root and two divisions. The computation of the auxiliary loading source $\tilde{F}$ requires $N_{\mathrm{D}}+2$ more multiplications and $N_{\mathrm{D}}-1$ more additions, because $\frac{1}{1+M_R}\left(\frac{1}{R}\right)^{\frac{1}{2}}$, R and $x_i - y_i$ have already been calculated. Thus, the total number of flops required in computing the auxiliary sources $\tilde{Q}$ and $\tilde{F}$ is 8 and $2N_{\mathrm{D}}+1$, respectively. Therefore, the total number of flops required in computing step (i) for N_{L} Lagrangian points and N_{P} time steps is $(5N_{\mathrm{D}}+11)N_{\mathrm{L}}N_{\mathrm{P}}$.

In step (ii), for computing the uniform spaced auxiliary sources at each Lagrangian point and each step, the computation of the coefficient λ_1 in the linear interpolation requires two more flops, including one subtraction and one division. With the computed coefficient λ_1, computing the uniformly spaced time series $\tilde{Q}'_j$ requires four more flops, including one addition, one subtraction and two multiplications. The computation of the uniformly spaced time series $\tilde{F}'_j$ requires three more flops with the computed λ_1 and $1-\lambda_1$, including one addition and two multiplications. Thus, the total number of flops required in computing the uniformly spaced time series $\tilde{Q}'_j$ and $\tilde{F}'_j$ is 6 and 3, respectively. Therefore, the total number of flops required in computing step (ii) for N_{L} Lagrangian points and N_{P} time steps is $9N_{\mathrm{L}}N_{\mathrm{P}}$.

In step (iii), for transforming the uniformly spaced auxiliary sources to the frequency domain at each Lagrangian point, we count the flops of the FFT according to the widely used "radix-2" algorithm.[27] The required number of flops is $5\log_2 N_{\mathrm{P}}$. Therefore, the total number of flops required in computing step (iii) for N_{L} Lagrangian points and N_{P} frequencies is $5N_{\mathrm{L}}N_{\mathrm{P}}\log_2 N_{\mathrm{P}}$.

In step (iv), the boundary integration of the frequency-domain auxiliary sources $\mathcal{F}(\tilde{F})$ and $\mathcal{F}(\tilde{Q})$ requires one addition and multiplication for each frequency at each Lagrangian point. We neglect the flops required for the multiplication between the boundary integration

and the coefficient $\frac{1}{4}\left(\frac{2\omega c_0}{\pi}\right)^{1/2} e^{\frac{\mathrm{i}\pi}{4}}$ for the thickness term and $\frac{-1}{4}\left(\frac{2\omega}{\pi c_0}\right)^{1/2} e^{\frac{\mathrm{i}\pi}{4}}$ for the loading term because the flops required for the multiplication is $2N_\mathrm{P}$ for all Lagrangian points and frequencies, which is negligible compared to the number for boundary integration. Therefore, the total number of flops required in computing step (iv) for N_L Lagrangian points and N_P frequencies is $4N_\mathrm{L}N_\mathrm{P}$.

Note that we have not accounted for the computation of sources $Q(\mathbf{y},t)$ and $F_i(\mathbf{y},t)$ in the above estimation. The computations of the thickness and loading sources $Q(\mathbf{y},t)$ and $F_i(\mathbf{y},t)$ require $2N_\mathrm{D}$ and $3N_\mathrm{D}$ flops, respectively. The required numbers of flops are estimated as follows. For the thickness source $Q=\rho v_i n_i$, the computation requires $N_\mathrm{D}-1$ additions and $N_\mathrm{D}+1$ multiplications. The computation of the loading source $F_i = pn_i + \rho v_i v_j n_j$ uses the result of the thickness source, thus leading to $3N_\mathrm{D}$ more flops, including $2N_\mathrm{D}$ multiplications and N_D additions. We have not taken these required flops into account because (1) the computations can be conducted in the sampling process, (2) both the proposed frequency-domain formulation and the conventional frequency-domain formulation require these computations, and (3) the required number of flops for computing these sources is negligible compared to that of the FFT.

Table A.2 presents the required number of flops for our proposed 3D formulation (Eqs. (25) and (26)). The difference between Table A.2 and Table A.1 lies in the distance decay factor in step (i), resulting from the distinction of the 2D and 3D Green's function.

Table A.3 presents the required number of flops for the conventional 2D formulation. Note that the computation of the integrand is also necessary for the conventional formulation. According to the work of Cooley and Tukey,[29] the direct use of the discretized Fourier transform (Eqs. (6) and (14)) includes one complex multiplication and one complex addition for each frequency at each Lagrangian point. The computation of the discretized Fourier transform thus requires $2(N_\mathrm{P}-1)N_\mathrm{L}N_\mathrm{P}$ additions, occupying most of the computational operations listed in Table A.3.

Table A.2. Flops required for the 2D formulation proposed in this work (Eqs. (25) and (26)).

Step order and symbol	Required computation	Number of flops	Total number of flops in each step
Step (i) (N_{R1})	$\tau = t + R/c_0$	$(3N_\mathrm{D}+2)N_\mathrm{L}N_\mathrm{P}$	$(5N_\mathrm{D}+10)\ N_\mathrm{L}N_\mathrm{P}$
	$\tilde{Q} = \frac{Q}{1+M_R}\left(\frac{1}{R}\right)$	$7N_\mathrm{L}N_\mathrm{P}$	
	$\tilde{F} = \frac{F_i(y_i-x_i)}{1+M_R}\left(\frac{1}{R}\right)^2$	$(2N_\mathrm{D}+1)N_\mathrm{L}N_\mathrm{P}$	
Step (ii) (N_{FI1})	$\tilde{Q}'_j = \tilde{Q}_i\lambda_1 + \tilde{Q}_{i+1}(1-\lambda_1)$	$6N_\mathrm{L}N_\mathrm{P}$	$9N_\mathrm{L}N_\mathrm{P}$
	$\tilde{F}'_j = \tilde{F}_i\lambda_1 + \tilde{F}_{i+1}(1-\lambda_1)$	$3N_\mathrm{L}N_\mathrm{P}$	
Step (iii) (N_{FT1}, N_{FL1})	fast Fourier transform of $\tilde{Q}'$	$5N_\mathrm{L}N_\mathrm{P}\log_2 N_\mathrm{P}$	$10N_\mathrm{L}N_\mathrm{P}\ \log_2 N_\mathrm{P}$
	fast Fourier transform of $\tilde{F}'$	$5N_\mathrm{L}N_\mathrm{P}\log_2 N_\mathrm{P}$	
Step (iv) (N_{IT1}, N_{IL1})	surface integration of $\mathcal{F}(\tilde{Q}')$	$2N_\mathrm{L}N_\mathrm{P}$	$4N_\mathrm{L}N_\mathrm{P}$
	surface integration of $\mathcal{F}(\tilde{F}')$	$2N_\mathrm{L}N_\mathrm{P}$	

Table A.3. Flops required for the conventional 2D formulation (Eqs. (6) and (14)).

Step order and symbol	Required computation	Number of flops	Total number of flops in each step
Step (i) (N_{R2})	$\tau = t + R/c_0$	$(3N_{\mathrm{D}} + 2)\ N_{\mathrm{L}}N_{\mathrm{P}}$	$(5N_{\mathrm{D}} + 11)\ N_{\mathrm{L}}N_{\mathrm{P}}$
	$\tilde{Q} = \frac{Q}{1+M_R}\left(\frac{1}{R}\right)^{\frac{1}{2}}$	$8N_{\mathrm{L}}N_{\mathrm{P}}$	
	$\tilde{F} = \frac{F_i(y_i - x_i)}{1+M_R}\left(\frac{1}{R}\right)^{\frac{3}{2}}$	$(2N_{\mathrm{D}} + 1)\ N_{\mathrm{L}}N_{\mathrm{P}}$	
Step (ii) (N_{FI2})	—	—	—
	—	—	
Step (iii) (N_{FT2}, N_{FL2})	discretized Fourier transform of thickness sources	$2(N_{\mathrm{P}} - 1)\ N_{\mathrm{L}}N_{\mathrm{P}}$	$4(N_{\mathrm{P}} - 1)\ N_{\mathrm{L}}N_{\mathrm{P}}$
	discretized Fourier transform of loading sources	$2(N_{\mathrm{P}} - 1)\ N_{\mathrm{L}}N_{\mathrm{P}}$	
Step (iv) (N_{IT2}, N_{IL2})	boundary integration of thickness sources	$2N_{\mathrm{L}}N_{\mathrm{P}}$	$4N_{\mathrm{L}}N_{\mathrm{P}}$
	boundary integration of loading sources	$2N_{\mathrm{L}}N_{\mathrm{P}}$	

Table A.4. Flops required for the conventional 3D formulation (Eqs. (6) and (14)).

Step order and symbol	Required computation	Number of flops	Total number of flops in each step
Step (i) (N_{R2})	$\tau = t + R/c_0$	$(3N_{\mathrm{D}} + 2)\ N_{\mathrm{L}}N_{\mathrm{P}}$	$(5N_{\mathrm{D}} + 10)\ N_{\mathrm{L}}N_{\mathrm{P}}$
	$\tilde{Q} = \frac{Q}{1+M_R}\left(\frac{1}{R}\right)$	$7N_{\mathrm{L}}N_{\mathrm{P}}$	
	$\tilde{F} = \frac{F_i(y_i - x_i)}{1+M_R}\left(\frac{1}{R}\right)^2$	$(2N_{\mathrm{D}} + 1)\ N_{\mathrm{L}}N_{\mathrm{P}}$	
Step (ii) (N_{FI2})	—	—	—
	—	—	
Step (iii) (N_{FT2}, N_{FL2})	discretized Fourier transform of thickness sources	$2(N_{\mathrm{P}} - 1)\ N_{\mathrm{L}}N_{\mathrm{P}}$	$4(N_{\mathrm{P}} - 1)\ N_{\mathrm{L}}N_{\mathrm{P}}$
	discretized Fourier transform of loading sources	$2(N_{\mathrm{P}} - 1)\ N_{\mathrm{L}}N_{\mathrm{P}}$	
Step (iv) (N_{IT2}, N_{IL2})	surface integration of thickness sources	$2N_{\mathrm{L}}N_{\mathrm{P}}$	$4N_{\mathrm{L}}N_{\mathrm{P}}$
	surface integration of loading sources	$2N_{\mathrm{L}}N_{\mathrm{P}}$	

Table A.4 presents the required number of flops for the conventional 3D formulation (Eqs. (6) and (14)). The difference between Table A.4 and Table A.3 lies in the distance decay factor in step (i), resulting from the distinction of the 2D and 3D Green's functions.

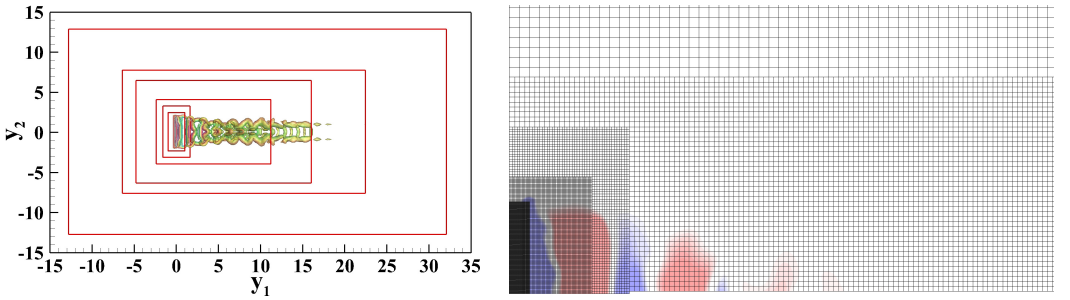

(a) (b)

Fig. B.1. Schematic of the computational domain from the top view: (a) boundaries of six levels of refinement; and (b) unstructured Cartesian mesh with hanging nodes.

Appendix B. Numerical Methods and Setups for the Flapping Rectangular Wing

The flapping rectangular wing model, detailed in Sec. 4.2, provided the sound source field for comparing the efficiency of the proposed method with that of the conventional frequency-domain FW-H integral. The sound source field was obtained by numerically solving the incompressible Navier–Stokes equation:

$$\begin{aligned} \frac{\partial u_i}{\partial t} + u_j \frac{\partial u_j}{\partial y_i} &= -\frac{1}{\rho_0}\frac{\partial p}{\partial y_i} + \nu \frac{\partial u_i}{\partial y_j \partial y_j}, \\ \frac{\partial u_j}{\partial y_j} &= 0. \end{aligned} \tag{B.1}$$

The exact projection method is employed to decouple the pressure and velocity fields. A second-order finite method based on an unstructured Cartesian mesh with hanging nodes is used to discretize the computational domain and the three-step second-order Runge–Kutta method is used to advance in the time direction. More details can be found in our previous work.[30–32]

The computational domain is $[-12.8l_c, 32.0l_c] \times [-12.8l_c, 12.8l_c] \times [-19.2l_c, 19.2l_c]$ where l_c is the chord length of the flapping wing. The nonslip boundary condition is used on the wing surface. A uniform flow with velocity $U = 1\,\mathrm{m/s}$ is specified at the inlet. The free convection boundary condition is applied at the outlet. The slip boundary condition is used for the remaining boundaries. A Cartesian unstructured mesh with six levels of refinement is used, as shown in Fig. B.1. The minimum grid size of the mesh is $\mathrm{d}h = 0.02l_c$ and the total number of discretized cells is 5.07 million. The time step is $0.005U_f/l_c$. The initial velocity over the computational domain is $\mathbf{u} = (U_f, 0, 0)$.